Research papers

Effect of surfactant on functionalized multi-walled carbon nano tubes enhanced salt hydrate phase change material

Reji Kumar R [a], A.K. Pandey [b,c,*], M. Samykano [a,**], Yogeshwar Nath Mishra [d,e], R.V. Mohan [f], Kamal Sharma [g], V.V. Tyagi [h]

[a] Faculty of Mechanical & Automotive Engineering Technology, Universiti Malaysia Pahang, 26600 Pekan, Pahang, Malaysia
[b] Research Centre for Nano-Materials and Energy Technology (RCNMET), School of Engineering and Technology, Sunway University, No. 5, Jalan Universiti, Bandar Sunway, Petaling Jaya 47500, Selangor Darul Ehsan, Malaysia
[c] Center for Transdisciplinary Research (CFTR), Saveetha Institute of Medical and Technical Sciences, Saveetha University, Chennai, India
[d] NASA-Jet Propulsion Laboratory, California Institute of Technology, California 91109, USA
[e] Department of Physics, University of Gothenburg, SE 41296 Gothenburg, Sweden
[f] Joint School of Nanoscience & Nanoengineering, North Carolina A&T State University, 27401 Greensboro, NC, USA
[g] Department of Mechanical Engineering, Institute of Engineering and Technology, GLA University, Mathura 281406, India
[h] School of Energy Management, Shri Mata Vaishno Devi University, Katra 182320, J&K, India

ARTICLE INFO

ABSTRACT

Phase change materials (PCMs) are effective thermal energy storage materials; however, their low thermal conductivity nature tends to affect heat storage performance. Salt hydrate being inexpensive, incombustible and ensuring high phase change enthalpy, are highly attractive for energy storage. The potential of multi-walled carbon nanotubes (MWCNTs) in improving the thermophysical properties of salt hydrate PCMs makes it a hotspot of current research. Therefore, in this research article, MWCNTs and functionalized multi-walled carbon nanotubes (FMWCNTs) nanoparticles were dispersed with inorganic salt hydrate at different concentrations (0.3, 0.5, and 1.0 wt%), in the presence and absence of surfactant. The role of surfactant with salt hydrate PCM has been discussed extensively. The results obtained have ensured an enhancement in melting enthalpy of prepared composites by 4.92 %, and 28.5 % for 0.5 wt% MWCNT dispersed PCM (SHM0.5), and 0.5 wt% FMWCNT dispersed PCM (SHF0.5), respectively. Furthermore, the maximum thermal conductivity was enhanced by 50.0 % and 84.78 % for 0.5 wt% MWCNT dispersed PCM with surfactant (SHMS0.5), and SHF0.5 respectively, compared to salt hydrate PCM. From the improvement in thermal conductivity, light absorptance, thermal stability, latent heat, and chemical stability, it is evident that the prepared nanocomposite is a potential candidate for solar thermal energy storage applications.

1. Introduction

The energy demand is increasing due to the increase of population, rapid industrialization, change in life style, technological developments etc. Today, most energy demands are met by burning fossil fuels such as natural gas, coal, crude oil, etc., which is not a sustainable or renewable energy source. Studies have clearly shown that fossil fuel shortage will be unavoidable in 70 to 100 years due to its greater usage for over 200 years [1,2]. Therefore, alternate energy sources are required to fulfil the global energy requirement and minimize the globate climate issues.

Different types of renewable energies are available like wind, solar, tidal, geothermal energy, [3]; these energies have promising applications and potential to fulfil the required energy demand without polluting the environment. Out of all renewable energies, solar energy is one of the most promising, environment-friendly and abundant source of energy. However, the solar energy can be harnessed only in the day time as it is intermittent in nature and proper method of its storage is required to make the solar energy technology more viable and user friendly [4]. Thermal energy storage (TES) is an extensively used energy storage (ES) technique in different energy conversion and management [5]. Phase Change Materials (PCMs) are one of the most attractive latent

---

Nomenclature

Nanocomposite codes

SH	salt hydrates (PlusICE-S50) phase change materials
SHM	MWCNT dispersed PCM
SHF	FMWCNT dispersed PCM
SHMS	MWCNT dispersed PCM with surfactant
SHFS	FMWCNT dispersed PCM with surfactant
SHM0.3	0.3wt%MWCNT dispersed PCM
SHM0.5	0.5wt%MWCNT dispersed PCM
SHM1.0	1.0wt%MWCNT dispersed PCM
SHF0.3	0.3wt%FMWCNT dispersed PCM
SHF0.5	0.5wt%FMWCNT dispersed PCM
SHF1.0	1.0wt%FMWCNT dispersed PCM
SHMS0.3	0.3wt%MWCNT dispersed PCM with surfactant
SHMS0.5	0.5wt%MWCNT dispersed PCM with surfactant
SHMS1.0	1.0wt%MWCNT dispersed PCM with surfactant
SHFS0.3	0.3wt%FMWCNT dispersed PCM with surfactant
SHFS0.5	0.5wt%FMWCNT dispersed PCM with surfactant
SHFS1.0	1.0wt%FMWCNT dispersed PCM with surfactant

Abbreviations

DSC	differential scanning calorimetry
TGA	Thermo Gravimetric Analysis
FT-IR	Fourier transmission Infrared
UV–Vis	Ultraviolet Visible Spectrum
TEM	transmission electron microscopy
$[Ni(NH_3)_6](NO_3)_2$	nickel nitrate hexamine
Al_2O_3	aluminum dioxide
Fe_2O_3	iron oxide
SiO_2	silicon dioxide

TiO_2	titanium dioxide
PCM	Phase Change Materials
PV	photovoltaic
TES	thermal energy storage
NePCMs	Nano enhanced Phase Change Materials
MWCNTs	multi walled carbon nanotubes
SDBS	sodium dodecyl benzene sulfonate
FMWCNTs	functionalized multi walled carbon nanotubes
TEM	transmission electron microscopy
TC	thermal conductivity
LH	latent heat
DMF	di-methyl formamide
CBNP	carbon black nano powder
PIT	phase inversion temperature
PE-b-PEG	Polyethylene-block-Polyethylene glycol
HVAC	heating ventilation and air conditioning
xGnP	exfoliated graphene nanoplatelets
MgO	magnesium oxide
CSM	ceramic skeleton materials
GA	graphene aerogel
NPs	nanoparticles
CNTs	carbon nanotubes
ES	energy storage

List of symbols

k	thermal conductivity ($Wm^{-1}K^{-1}$)
T	temperature in (°C)
t	time in s
μ	microns
g	grafted

heat (LH) storage materials [6,7]. Because of their diverse temperature range, wide-ranging thermophysical properties and low cost, inorganic salt hydrates are one of the widely used PCMs for TES applications [8,9]. The heat energy can be accumulated when the materials changes its phase from solid to liquid, and the stored heat energy can be released when the material changes its phase from liquid to solid at an almost constant temperature. PCM stores the heat energy when solar energy is available and releases the heat energy when solar energy is unavailable. The stored heat energy can be used for medium-temperature applications like water heating, industrial applications, dishwashing, heating, ventilation and air conditioning (HVAC), crop drying [10]. However, the major drawback of this PCMs is their low thermal conductivity (TC), leading to low heat transfer rate and TES ability [11]. To enhance the thermophysical performance of the PCM, researchers have suggested dispersing nanoparticles such as metallic particles, oxides [12] and carbon-based particles into the base PCM [13,14]. Further research [15,16] has shown that the dispersion of Functionalized multi-walled carbon nanotubes (FMWCNTs) in PCM gives excellent dispersion stability, thermal conductivity, light absorptance, thermal stability and life cycle. In addition, more studies [4,17,18] have confirmed that the addition of surfactant improves the dispersion capability and reduces the agglomeration of particles in PCM. For example, Graham et al. [19] reported that the inorganic Magnesium nitrate hexahydrate (Mg(NO$_3$)$_2$.6H$_2$O) is an excellent energy storage material with higher heat storage capacity and is a potential thermal energy storage material for TES applications. In addition, it was noticed that the LH decreased minimally after 100 thermal cycles. Ranjbar et al. [18] have studied the thermal performance and dispersion stability of multi-walled carbon nanotubes (MWCNTs) and FMWCNTs dispersed PCM for ES applications. It was seen that MWCNTs has excellent dispersion stability and thermophysical properties for non-polar PCMs like Paraffin wax, Steric

acid, etc. At the same time, surface modified MWCNT has outstanding properties in polyethylene glycol. Mayilvelnathan et al. [20] have studied the thermal performance of graphene nanoparticles (NPs) enhanced erythritol PCM for TES applications. It was noted that a remarkable improvement in TC by 53.1 % at 1.0 wt% graphene and the melting enthalpy was slightly decreased. In addition, the nanocomposites are thermally and chemically stable even after 100 heating and cooling cycles. Liu et al. [17] have performed experiments with nano dispersed highly stable PCM with surfactant, used for TES. It was stated that the developed nano dispersed PCM significantly decreases the supercooling effect. Furthermore, researcher used two different surfactants by phase inversion temperature method (PIT). Brij-4 as a main surfactant and Polyethylene-black-Polyethylene glycol (PE-b-PEG), or Tween-60 or Tween-80 as a secondary surfactant. The viscosity, droplet size, dispersion, PIT point and stability of these nano particles depends on the surfactant ratios. In addition, Pinto et al. reported that, the supercooling effect on salt hydrate PCMs can be reduced by adding nanoparticles [21].

Karaipekli et al. [22] have analyzed the expanded perlite/CNTs dispersed eicosane (C20) organic PCM for enhancing the thermo physical properties of PCM. It was observed dispersion of expanded perlite in C20 PCM had excellent thermal stability. And the use of CNTs improves the TC without disturbing the TES performance, and the thermal stability is higher than Exp/C20 nanocomposites. Chen et al. [23] described that the TC was increased by 54.1 % when using 5 wt% of MWCNTs. Also, it was noticed that the nanoparticle concentration increases with an increase in the TC. Mishra et al. [24] have studied Palmitic acid (PA)-dimethylformamide (DMF) PCM with four different nanoparticles like carbon black nanopowder, graphene nanoplatelets, multi-wall carbon nanotube and Aluminum dioxide (Al$_2$O$_3$) for TES applications. It was reported that carbon black nanoparticles (CBNP) have higher TC than

other metallic and carbon nanotubes. Harikrishnan et al. [25] have analyzed the thermophysical performance of stearic acid with titanium dioxide (TiO$_2$) nanoparticles. The results revealed that the TC increases with an increase in the weight concentration of NPs. Thermal conductivity was enhanced by 70.53 % when adding 0.3 wt% TiO$_2$ nanoparticles. The DSC results show that after adding TiO$_2$ NPs to the PCM, the solidification and melting temperatures were reduced in all concentrations. A step by step thermal degradation of inorganic PCMs, like Mg(NO$_3$)$_2$.6H$_2$O, nickel nitrate hexamine and [Mg(NH$_3$)$_6$](NO$_3$)$_2$, were analyzed by Mikuli et al. [26]. It was reported that the decomposition of Mg(NO$_3$)$_2$.6H$_2$O decomposes in two stages. The first stage shows decomposing of the hydrates around 60 °C to 300 °C, and the second stage decomposes magnesium nitrate around 450 °C; the remaining leftover is magnesium oxide & carbon residues. Again, the first stage breaks down into two steps; the first step decomposes 5H$_2$O, and in the next step, the remaining H$_2$O decomposes. Masoumi et al. [27] analyzed the performance of TiO$_2$ dispersed stearic acid PCM for TES applications. The developed nanocomposites had excellent thermophysical properties even after 250 cycles. It was described that the TC of developed NePCM was enhanced to 27 % more than pure stearic acid PCM. Daneshazarian et al. [28] have investigated exfoliated graphene nanoplatelets (xGnP) dispersed Octadecane PCM at various concentrations to enhance thermal properties. It was found that the melting temperature decreased by 9.7 %, and melting enthalpy increased by 12.6 %, respectively, at 0.5 wt % xGnP. The heat transfer performance of PCM depends on relative changes in thermophysical characteristics like viscosity, TC, LH, density and specific heat of PCM. Sandeep Kumar et al. [29] have investigated hybrid nanoparticles Al$_2$O$_3$ and copper oxide (CuO) dispersed with paraffin to increase the thermophysical performance of PCM. Researcher used the various mixing ratio 75:25, 50:50, and 25:75 at various weight concentrations (0.5 %, 1.0 %, 2.0 %, and 3.0 %) with paraffin wax. It was reported that excellent thermophysical properties were obtained at Al$_2$O$_3$:CuO (75:25) with paraffin at 2 wt% concentration. A magnesium oxide (MgO) and graphite flakes dispersed eutectic NaLiCO$_3$ PCM were prepared and characterized for TES applications [30]. The prepared nanocomposite had higher thermal conductivity, excellent mechanical strength, also found rigid structure even after thermal cycling. Singh et al. [31] have analyzed functionalized graphene nanoparticles dispersed eutectic PCM for efficient solar absorption and TES. The developed composite PCM's TC enhanced by 104 % than pure LiNO$_3$-KCl (50:50) eutectic PCM. The specific heat enhanced by 80 % than pure eutectic PCM in solid phase. Zhou et al. [32] have examined the properties of zinc oxide (ZnO) and graphene aerogel (GA) based polyurethane PCMs for energy harvesting, energy conversion management, etc. and reported an excellent improvement in latent heat from 86.8 to 108.1 kJ/kg. Further, the developed nanocomposite was found to be excellent in thermal stability, reliability, and photo-thermal conversion efficiency.

Thermophysical properties of an inorganic PCM with various metal oxide nanoparticles were investigated by Gupta et al. [33]. This research used magnesium nitrate hexahydrate as a PCM and TiO$_2$, Fe$_2$O$_3$, SiO$_2$, and ZnO as nanoparticles. The experimental outcome shows that the thermal conductivity of nano PCM composite increased by 147.5 %, 55 %, 62.5 %, and 45 % for 0.5 wt% of TiO$_2$, Fe$_2$O$_3$, ZnO, and SiO$_2$ respectively. The supercooling effect was decreased and the melting enthalpy was maintained in the range. A novel nanocarbon dispersed PCM was prepared for solar TES applications [34], in which nanographene and coconut shell charcoal nano powder were used as nanoparticles. Oleic acid and span- 80 were used as dispersants to minimize the agglomeration of nanocomposites. The TC was increased with an increase in nanoparticle weight concentration. There was no change in melting and solidification enthalpy, which is almost similar to base paraffin. The thermal performance of MWCNTs/graphene nanoplatelets enriched Polyethylene glycol-6000 was investigated for TES applications [35]. The TC was enhanced by 61.73 % and 84.48 % for MWCNT/PEG6000 and Graphene nanoplatelets/PEG-6000, respectively.

From the above literature, many researchers [18,28,30,35] reported that the adding nano-sized particles increase the thermal conductivity of PCMs, optical capabilities, and thermal stability; while, a few of the researchers [18,21,36,37] are formulated MWCNT and FMWCNTs dispersed PCM and the thermophysical properties were characterized. Ahmed et al. [36] studied the properties grafted MWCNT with Octadecanol PCM - the thermal conductivity was increased to 263 % and the latent heat reduces to 234.5 from 269.3 at 5.0 wt% MWCNTs. Pinto et al. [21] reported that, use of salt hydrate and NPs enhances the TC, phase segregation eradicated, and reduced the supercooling. Ranjbar et al. [18] studied and compared the properties of MWCNT and FMWCNT with three different PCMs viz. stearic acid, paraffin wax and polyethylene glycol. The results have shown that MWCNTs had higher stability with non-polar PCMs and FMWCNTs have higher stability in polar PCMs. As per above literature review and to the best of author's knowledge, a detailed study of the thermal performance of salt hydrate with MWCNT and FMWCNT with and without surfactant is hardly to be found in recent literature; also, there is no literature found on the effect of surfactant in salt hydrates PCM in the melting range of 50 °C with MWCNTs and FMWCNTs. Therefore, in this work, salt hydrates PCM with a melting point range of 50 °C, MWCNTs, and acid-treated MWCNT known as FMWCNT as nanoparticles and Sodium dodecylbenzene sulfate (SDBS) as surfactant/stabilizer were used. Additionally, the FMWCNTs nanoparticles were chosen because of their well-known higher dispersion stability, photocatalytic properties and reduced infrared transmittance. So, the novelty of the present work lies in reporting the effect of surfactant on MWCNT and FMWCNTs with salt hydrate and first time conducting the effect of surfactant in functionalized and non-functionalized MWCNT with salt hydrate PCM melting temperature in the range of 50 °C and comparing the thermophysical performance of developed composites. The objective of this research is to fabricate nanocomposites in different weight concentrations (0.3, 0.5, and 1.0 %) with and without surfactant and examine their thermal stability, TC, LH, light transmission, and thermal reliability of the developed composites. To ensure the thermal reliability of the nanocomposites a 500 thermal cycling was done. The results demonstrated that Salt hydrate with FMWCNT (SHF) has better TC, solar energy absorptions, melting enthalpy, and other thermal properties compared to salt hydrate with MWCNT (SHM), with MWCNT and surfactant (SHMS), and with FMWCNT and surfactant (SHFS) composites. This research has potential applications such as cooling of electronic components (40.2 °C to 80 °C) [38], solar desalination, household solar air and water heaters (38 °C to 78 °C) [39,40], pavement cooling (42 °C to 78 °C) [41], solar collectors (60 °C to 68 °C) [4], automotive cooling [42] and photovoltaic thermal systems (35 °C to 65 °C) [43].
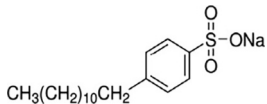
2. Materials and methods

2.1. Thermophysical properties of the used materials

High-grade inorganic salt hydrate PlusICE-S50 has been used as a PCM. It has a melting temperature of 50 °C (from supplier); therefore, it can be employed in solar thermal TES applications. The multi-wall carbon nanotube (MWCNT) has an average nanoparticle size of 10–20 nm outside diameter and 10–30 μm length (Cheap Tubes Inc., USA). SDBS was purchased Sigma-Aldrich (M) Sdn Bhd, and high-grade nitric and sulfuric acid were purchased from EMSURE, Germany; the acid concentrations were about 65 % and 97 %, respectively. The thermophysical performance of salt hydrate, MWCNTs, and SDBS are shown in Table 1.

2.2. Functionalization of MWCNTs

To begin with, a flask was filled with 0.5 g of MWCNT, followed by a mixture of H$_2$SO$_4$ and HNO$_3$. Next, the composition of the MWCNT and the chemicals were mixed using a bath sonicator for 1 h at room

Table 1

Properties of Salt hydrate PCM and MWCNTs.

Properties	Materials		
	PlusICE-S50	MWCNTs	SDBS
Thermal conductivity (k) in $Wm^{-1}K^{-1}$	0.44	2990	–
Phase transition temperature °C	50	3649–3696	204–207
Heating enthalpy J/g	100	–	–
Color	White	Black	White
Surface area m^2/g	–	216	–
Density g/mol	–	2.1	0.18
Appearance	–	–	Flake
Molecular weight g/mol	–	–	348.48
Size	–	Outer Diameter (D0): 10–20 nm Length (l): 10–30 μm Purity: >95 wt%	
Molecular structure	–	–	$CH_3(CH_2)_{10}CH_2$—⟨benzene ring⟩—SO_2—ONa

temperature. In addition, the composition mixture was refluxed for 24 h at 65–70 °C at 300 rpm. Furthermore, the solution was diluted with distilled water and centrifuged several times to reach the solution pH value of 5.5. Later the solution is dried using a vacuum oven for 12 h at 50 °C temperature and 100 mbar pressure. Finally, COOH group compounds were added to MWCNT and were investigated further.

2.3. Fabrication of nano-enhanced PCM with and without surfactant

The MWCNT/SH and FMWCNT/SH PCMs were developed by dispersing various weight % of nanoparticles in pure PCM. In this investigation, various weight concentrations like 0.3, 0.5, and 1.0 wt% MWCNTs were dispersed into salt hydrate PCM. The NePCMs were developed using the two-step method, as shown in Fig. 1. In this method, a conical flask with salt hydrate PCM was placed on the hot plate and

stirred and heated above the melting point by adding the required wt% surfactant (SDBS). The mixture was sonicated for 1 h by adding MWCNTs, ensuring the temperature was not less than the melting point to get good dispersion and avoid the agglomeration of nanoparticles. A similar method was adopted by preparing various concentrations (0.3, 0.5, and 1.0 wt%) of MWCNT without surfactant, MWCNT with a surfactant, FMWCNT without surfactant, FMWCNT with surfactant.

2.4. Characterization techniques

Thermal properties analyzer (TEMPOS Thermal analyzer SH-3, METER Group) was used to determine the TC of PCM nanocomposites at room temperature with a measurement of about ±5 %. Transmission electron microscope (TEM) (Model: FEI Tecnai G2 20 TWIN Holland, 200 kV, emitter LaB6) was used to identify particle's structure, size as well as their distribution. It also analyzes the elemental mapping, lattices and fringes viewing and the diffraction pattern of particles and compounds. The chemical composition of the nanocomposite was examined by using Fourier transform infrared (FTIR); on a Perkin Elmer, instruments were taken in the transmittance mode with 64 scans to 4000 cm^{-1} from 400 cm^{-1}. The thermal degradation behaviour of salt hydrate and nano PCM was determined using Thermogravimetric analyser (TGA). Measurements were taken from 28–30 °C to 650 °C, with a ramp of 10 °C/min under N_2 atm. The stability was performed by using Perkin Elmer TGA-4000. The enthalpy, melting, and freezing temperature of salt hydrate and its nanocomposites were examined by differential scanning calorimetry (DSC). DSC has performed 100 thermal cycles in N_2 atm with a ramp of 5 °C/min between 30 and 120 °C, using DSC-1000/°C. The light transmission of prepared nanocomposite was evaluated by LAMBDA-750, ranging from 220 nm to 2000 nm. The elemental analysis and elemental mapping of the developed nanocomposites were assessed by Energy Dispersive X-ray Spectroscopy (EDX) (Model: K-Max,880, Oxford Instrument). Using a large electric current allows short time analysis without degrading the quality of analysis accuracy or elemental map.

3. Results and discussion

3.1. Morphological behaviour

The TEM image in Fig. 2 shows the microstructure and morphology of pristine MWCNTs and FMWCNTs. Initially, the size of MWCNT is noted between 10 and 20 nm, and prior to acid functionalization, the size of the MWCNT is slightly increased; almost the same result was reported by Le et al. [44]. Furthermore, the FMWCNTs looks straight

Fig. 1. Fabrication method of nano-enhanced PCM with and without surfactant.
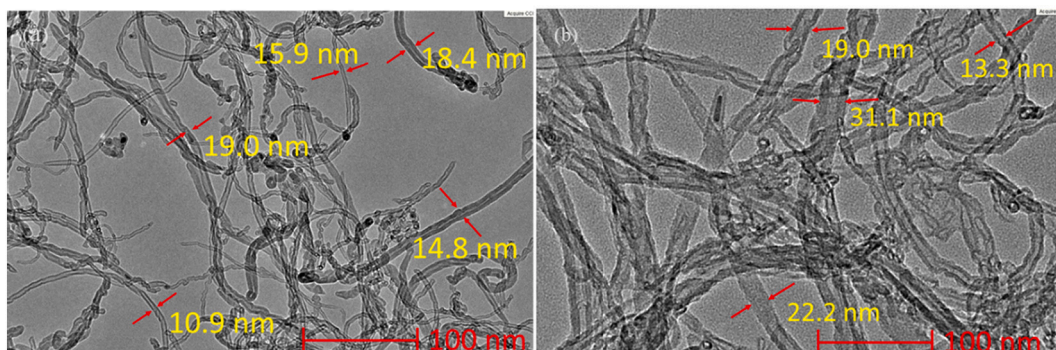
Fig. 2. TEM images of (a) MWCNTs (b) FMWCNTs.

and have more smooth surfaces than pristine MWCNT. Results, the COOH group is attached to the surface of the MWCNTs. The EDX analysis examined the prepared composite's homogeneity and establishes several dominating elements. A high-quality result was obtained by transmitting the X-ray emitted by the detector, which is plotted on the Y-axis concerning the energy level of the counts as gauged in the X-axis in keV. The EDX image of salt hydrate PCM in weight % and atomic % of N, O, Mg were 23.93 %, 68.99 %, 7.08 %, and 27.07 %, 68.32 %, 4.61 %,
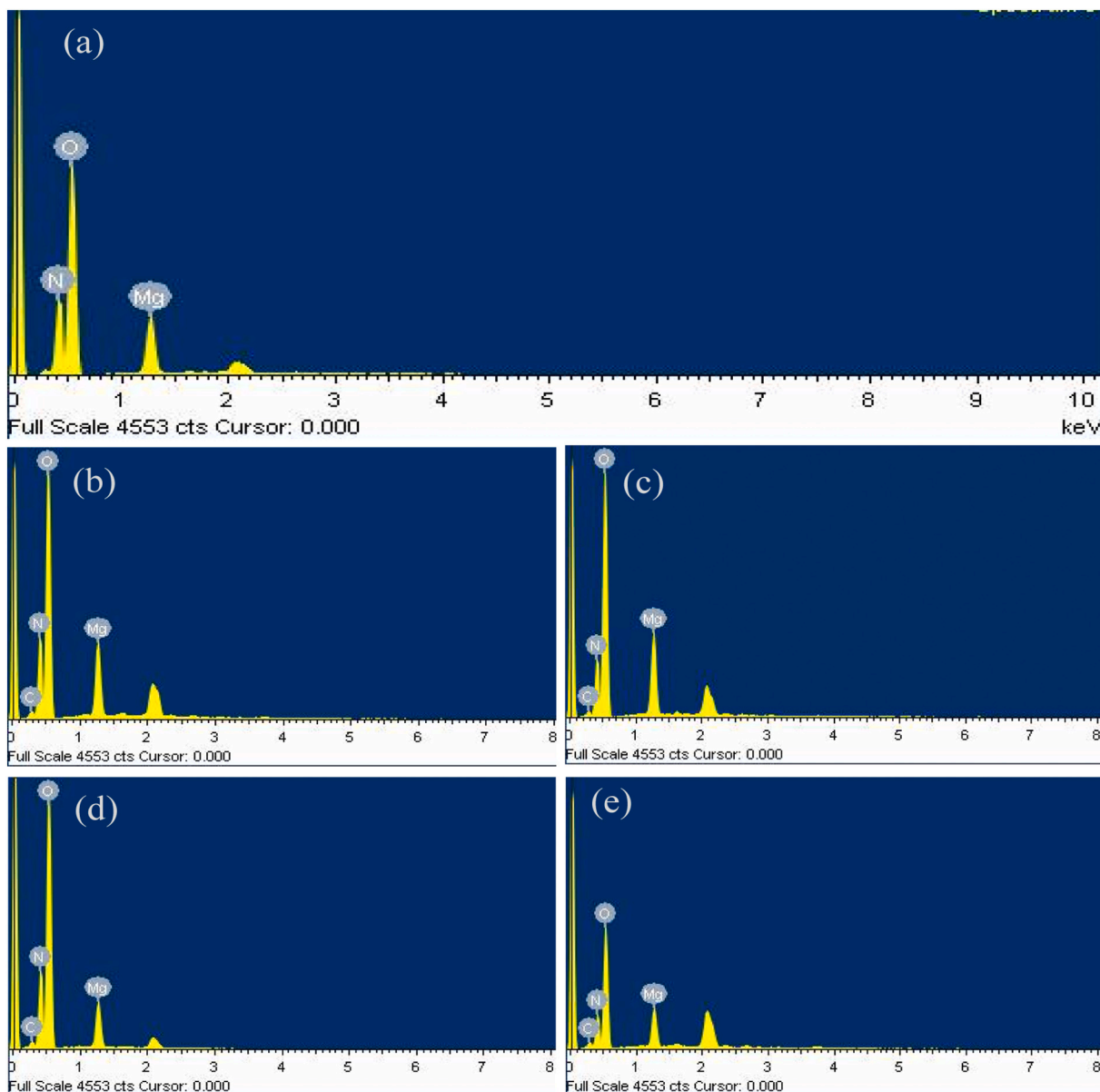

Fig. 3. FESEM-EDX analysis-Percentage of elements (a) SH, (b) SHM1.0, (c) SHMS1.0, (d) SHF1.0, (e) SHFS1.0.

respectively. It is obvious from the image that carbon elements not appeared in the PCM. The weight percentage of SHM1.0 composites for N, O, Mg and C are 22.87 %, 67.75 %, 7.34 %, and 2.05 %, respectively. Similarly, the weight % of SHMS1.0 composites for N, O, Mg and C are 19.71 %, 68.99 %, 9.51 %, and 1.79 %, respectively. Correspondingly, the weight % of SHF1.0 composites for N, O, Mg and C were 23.35 %, 68.65 %, 6.39 %, and 1.61 %, respectively. Conversely, the weight % of SHFS1.0 composites for N, O, Mg, and C are 21.26 %, 66 %, 7.93 %, and 3.7 %, respectively, while testing with a maximum intensity of 10 keV. The tested EDX spectrum of SH/MWCNT/FMWCNT composites is shown in Fig. 3(a)–(e), evidently showing the carbon particles and magnesium nitrate hexahydrate. The results confirmed that carbon particles exist in the prepared SHM1.0, SHMS1.0, SHF1.0, and SHFS1.0 nanocomposites. Also, there was not much difference in elements present with surfactant and without surfactant in the composite due to a very less amount of SDBS added in the composites.

Furthermore, the FESEM-EDX spectrum of MWCNTs and FMWCNTs embedded salt hydrate PCM with surfactant and without surfactant have revealed the same peak of N, O, Mg, and C mostly from respective carbon-based materials and pure salt hydrate PCM. There were no other elements related to impurities that appear in the spectrum. To ensure the dispersion of MWCNT and FMWCNT with salt hydrate matrix, elemental mapping was performed. The elemental analysis of SHF1.0 was demonstrated in Fig. 4(a)–(d). It was obvious from the figures that the dopant was well disseminated in base PCM.

3.2. Nanocomposite chemical composition

In nature, MWCNT has a very weak peak of C=C aromatic ring that stretch at the wavelength of 1600 cm^{-1} [44]. Fig. 5 illustrates the FTIR graph of MWCNTs and FMWCNTs functional peaks at different wavenumbers. The graph shows 2 different bands, placed at 3224 cm^{-1} & 1623 cm^{-1}. The wavelength band at 3224 cm^{-1} ensure the stretching of hydroxyl group (-OH) from phenol group and carboxylic group
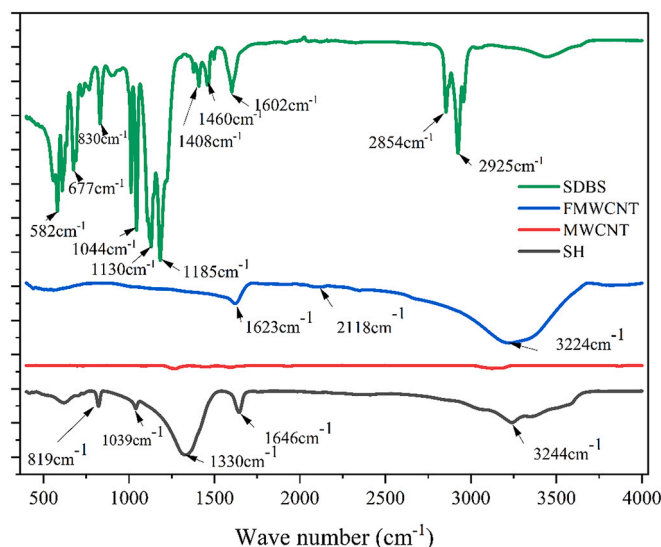
Fig. 5. FTIR results of Salt hydrate PCM, SDBS, MWCNT and FMWCNT.

(-COOH), while the wavelength band at 1623 cm^{-1} identified as the carbonyl (C=O) absorption, overlapped with (C=C) representing the backbone of CNTs [45]. From the graph ensures MWCNTs show a peak at wavelength 2345 cm^{1}, which illustrates the structure of CNTs; the same peak decreased and is represented in the FMWCNTs FTIR curve. It implied that the bond is broken and added new functional group. In addition, the peak should exist to make sure that MWCNT and no fatal damage after surface modification. However, the stretching of carbonyl (C=O) band would be influenced by carboxyl group (-COOH) linked with outside structure of MWCNTs. A tiny peak 2116 cm^{-1} denotes -OH group stretched from H-bond-COOH [46]. Moreover, a tiny peak is
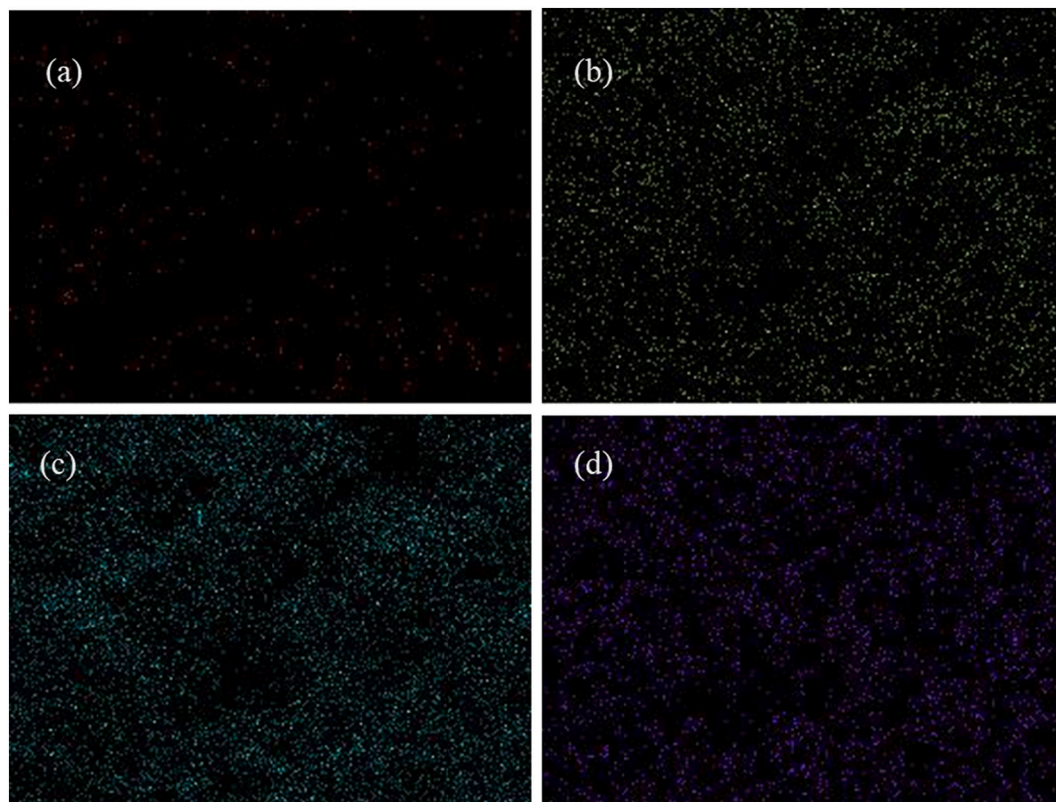
Fig. 4. FESEM-EDX elemental mapping of SH/FMWCNT composite (a) C, (b) N, (c) O, and (d) Mg.

observed between wavelength 1000 cm^{-1} and 1400 cm^{-1}, which displayed the presence of O—H from hydroxyl groups [44]. The peaks indicated the strong attachment of COOH group to MWCNT surfaces. The FTIR spectrum curve of SH has distinctive peaks for O—H stretching at 3244 cm^{-1}, N=O bending at 1646 cm^{-1}, a mixture of N—O stretching and bending of N=O at 1330 cm^{-1} and a sharp peak for NO^{3-} at 819 cm^{-1}.

The FTIR mainly analyzes the advancement of new bonds and functional groups of SHM and SHMS, as shown in Fig. 6(a) and (b). The FTIR spectrum of salt hydrate has distinctive peaks for O—H stretching at 3244 cm^{-1}, N=O bending at 1646 cm^{-1}, a combination of N—O stretching and bending of N=O at 1330 cm^{-1} and a sharp peak for NO$_3^-$ at 819 cm^{-1}. No sudden peaks or shifts are found in NePCM with surfactant and without surfactant compared with salt hydrate PCM. This obviously has shown that there was no chemical reactivity among salt hydrate PCM and MWCNT nanoparticles, and the nanoparticles and salt hydrate PCM were purely physically mixed and formed a stable composite. Similar findings were described by Wu et al. [47]. Also, the characteristic peak for O—H stretching at 3244 cm^{-1} confirmed unsaturated or aromatic compounds. Similarly, the FTIR spectrum of SH, SHF, SHFS for all weight percentages is displayed in Fig. 6(c) and (d). A long characteristic peak for O—H is stretching at 3244 cm^{-1}, N=O bending at 1330 cm^{-1}, along with C—O peaks at 1030 cm^{-1}, and a sharp peak NO$_3^-$ at 819 cm^{-1}. It was observed that the composites were physically mixed together, and there were no new peaks obtained compared to base PCM. This confirmed that the prepared nano dispersed PCM composite was chemically stable. The absorption bond 3244 cm^{-1} indicates the existence of O—H bond. It confirms the occurrence of aromatic or unsaturated compounds [47]. From the above discussion, it is evident that all the composites were physically well mixed, and no additional peaks were obtained in all samples. So, the prepared nanoparticle dispersed PCMs were found to be good for solar TES applications.

3.3. Latent heat capacity analysis

DSC analysis determines the impact of MWCNT and FMWCNT particle addition on the thermophysical property of salt hydrate PCM, containing the phase transition temperature and LH. The downward peak indicated the melting of PCM from solid-liquid. The sensible heat storage (solid to solid) occurs in the range of 32–40 °C. The DSC curve of pure salt hydrate PCM shows the phase transition appears onset at 40 °C and ends at 56–58 °C. The curve area below the phase change peak is considered to determine LH of salt hydrates. The LH capacity of base PCM was found to be 93.4 J/g and the melting temperature was 49.6 °C. The phase-changing temperature was computed by draw a tangent on the left side slope drawn across the peak of the graph. Fig. 7(a) shows the DSC graph of PCM with distinct weight concentration of 0.3, 0.5, and 1.0 % MWCNTs. The onset phase transition temperature started at 42.0 °C and ends at a range of 56–60 °C; the melting enthalpy was found at 98, 92, and 78 kJ/kg for SHM0.3, SHM0.5, SHM1.0, respectively. At a lower concentration, the latent heat increased, but the LH decreasing trend at higher concentration. The melting temperatures were also found to be having a slightly increasing trend. Similarly, Fig. 7(b) presents the DSC graph of salt hydrate PCM with various weight
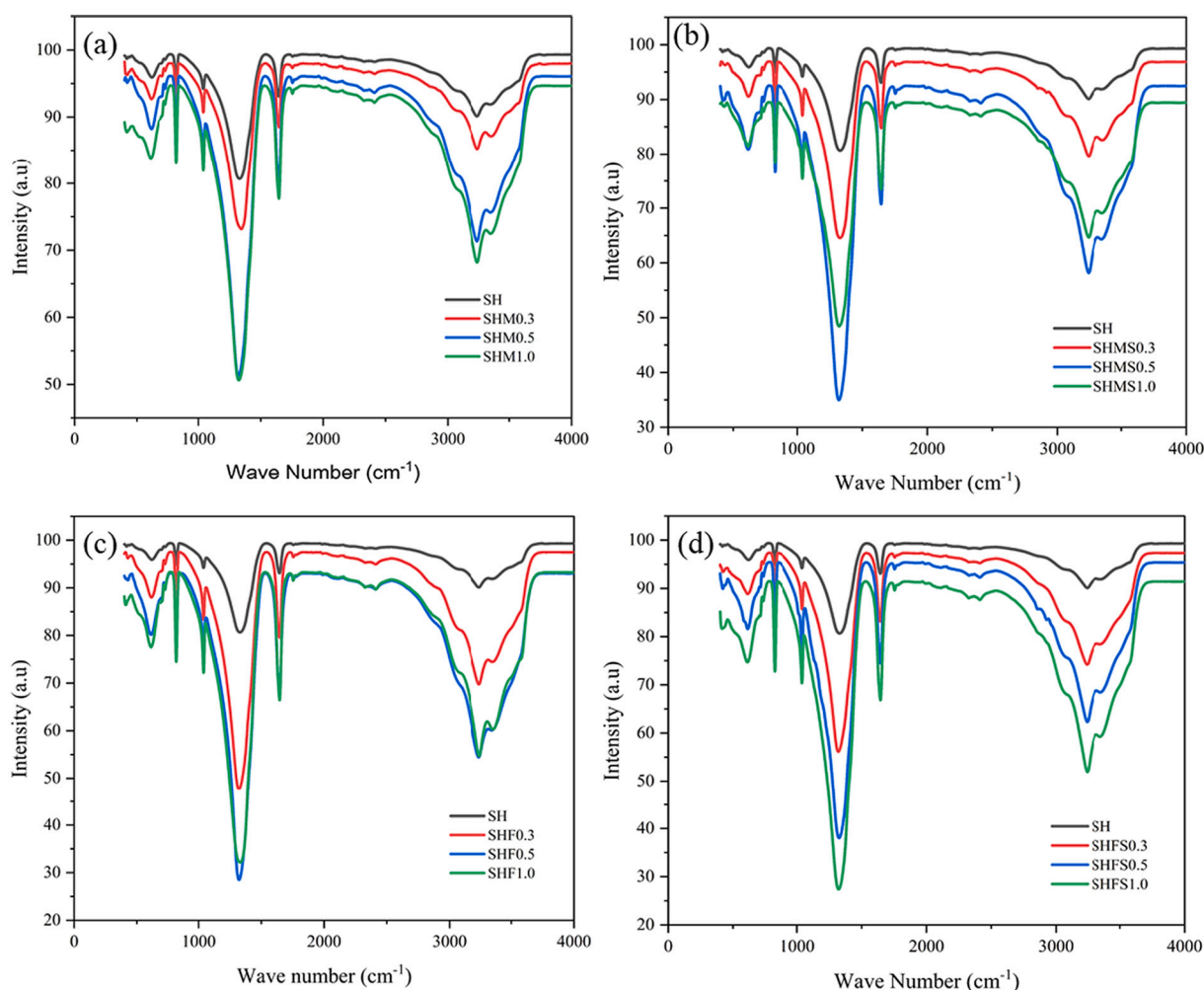

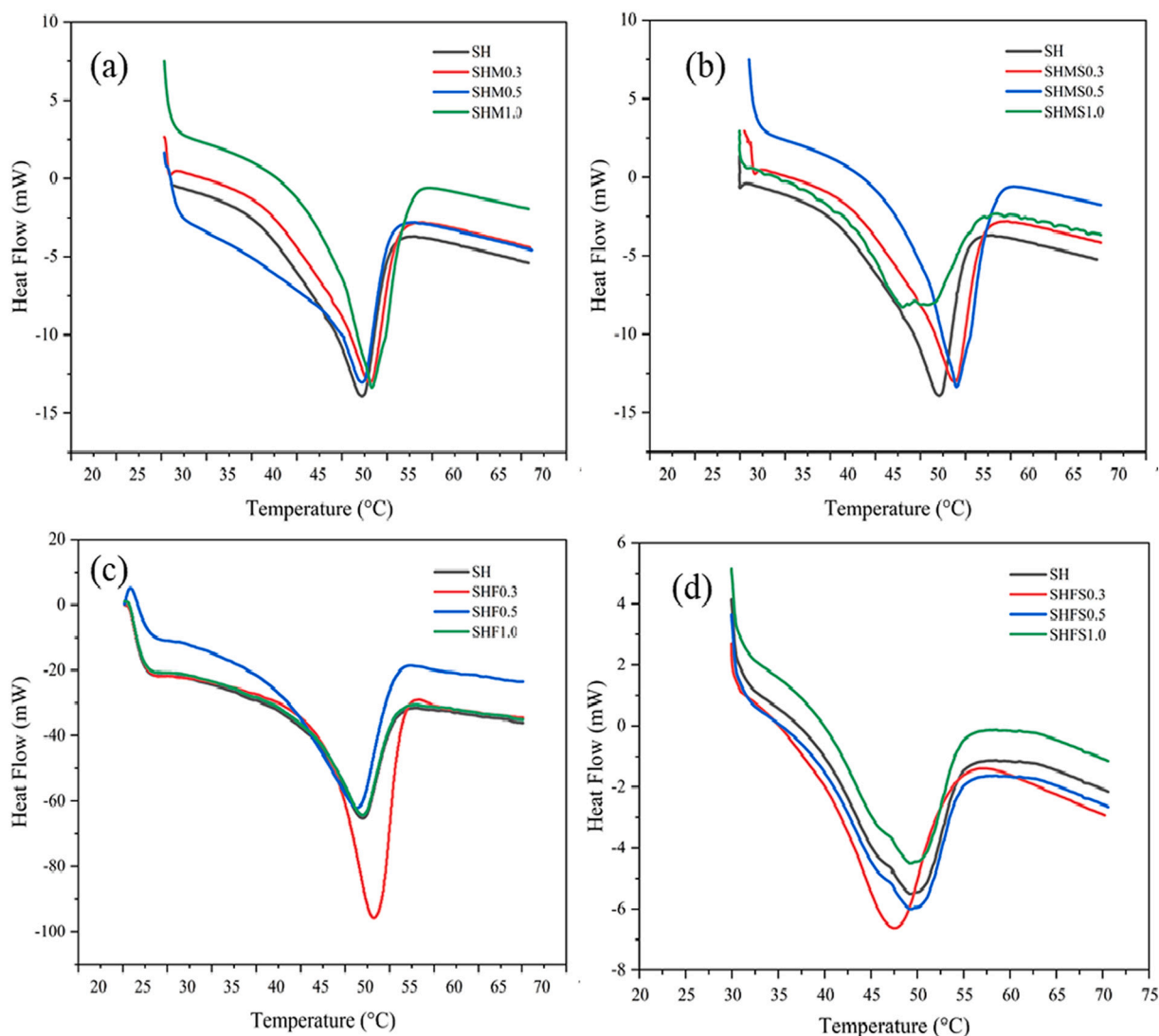**Fig. 6.** FT-IR results of SH and its composites (a) SHM, (b) SHMS (c) SHF (d) SHFS.

Fig. 7. Latent heat of prepared composites at various percentages (a) SHM, (b) SHMS, (c) SHF, (d) SHFS.

concentrations of 0.3, 0.5, and 1.0 % MWCNTs with SDBS. The onset phase shift occurred at 40 °C and ends at 55–58 °C, and the measured LH were 92, 88, and 78 kJ/kg for SHMS0.3, SHMS0.5, SHMS1.0, respectively. It was found that the latent heat increases at a lower concentration, but at higher concentrations, it showed a decreasing trend. The melting temperatures were found to be shaving lightly increasing trend, except for SHMS1.0 composites.

Similarly, the DSC graph of salt hydrate PCM with several percentages of FMWCNTs is displayed in Fig. 7(c). The onset phase transition temperature starts at 39 °C and ends at 56–60.5 °C and the measured LH are 120, 97.22, and 78 kJ/kg for SHF0.3, SHF0.5, and SHF1.0, respectively. It was found that the latent heat increased at lower concentrations and decreased at higher concentrations. The melting temperatures were slightly increased for all composites, except SHF1.0 composite; also, Fig. 7(d) exhibits the DSC graph of salt hydrate PCM with various weight concentrations of FMWCNTs with SDBS. The onset phase transition temperature occurs at 37 °C and ends at 57–61 °C, and the measured LH were 101, 96, and 75 kJ/kg for SHFS0.3, SHFS0.5, and SHFS1.0, respectively. It was found that the latent heat increases at lower concentrations, but it decreased at higher concentrations. The melting temperatures were also found to be slightly increasing in all composites than pure salt hydrate PCM. The melting points of all composites were found to be largely identical to those of base PCM. This

could be due to the nature of contact between PCM and the nanoparticles and the isotropic porous structure of carbon nanotubes. Further, it was because of the significant interaction between the fluid and the matrix's surface, resulting in a melting temperature shift. Similar findings are reported by Hari Krishnan et al. [48]. Due to their increased stability, FMWCNT dispersed PCM melted at a greater temperature than pristine MWCNT embedded PCM.

It is observed that the higher content of nanoparticle embedded PCM, latent heat was decreasing in all cases because the presence of the unchangeable solid nanocarbons and in case of a lower percentage of nanoparticles, the latent heat improved. The maximum increment in LH was observed at 98 kJ/kg, 120 kJ/kg and 101 kJ/kg, and the corresponding melting temperatures were 52.6 °C, 52.5 °C, and 46 °C for SHM0.3, SHF0.3, and SHFS0.3, respectively. The improvement in LH may be due to the interaction among the NPs and PCM. This may be due to the greater surface area of NPs between salt hydrate PCM and nanoparticles [49,50]. Also, higher molecular density of the MWCNT/ FMWCNT and its large surface area were the reasons behind the greater intermolecular attraction in the PCM and NPs, which resulted in their enhanced latent energy; the heat absorbed by the NPs and PCM may be greater than the intermolecular force among PCM particles [21]. A result, additional energy needs to be provided to the nanocomposites to convert them from solid phase to liquid phase. Indeed, the SHF

composites have a higher LH than SHM. The functionalization of MWCNT decreases the surface resistance and increased interaction between PCM and NPs. Furthermore, the heat of fusion increased with the addition of 0.3 wt% FMWCNT/FMWCNT with SDBS and decreased for higher content. This can be described by the thermodynamic formulae $dH = dU + VdP$ and $dU = TdS - PdV$. When FMWCNTs were dispersed into the salt hydrate PCM, the mixture tending to be in a chaotic state, and the entropy of PCM increased; for less content of NPs in the PCM, the increase in volume is negligible $TdS > PdV$ and $dU > 0$. On the basis of the relationship $dH = dU + VdP$, it was evident that $dH > 0$. Thus, the addition of less amount of NPs increased the LH, and the addition of higher content of NPs increased the volume of the nanocomposite; PdV would be increasing more than TdS, due to which dH and dU decreased [37]. Also, the surfactant/stabilizer reduced the LH in both cases due to the higher melting temperature of SDBS and the presence of unchangeable solid phase of SDBS. Moreover, FMWCNT dispersed PCM had higher melting enthalpy due to higher dispersion stability NPs in the PCM.

3.4. Light transmission capability

The photo transmissibility potential of pristine inorganic PCM with distinct weight concentrations of MWCNT composite were analyzed using an Ultraviolet Visible spectrometer (LAMBDA 750, Perkin Elmer) as depicted in Fig. 8(a) and (b). In solar thermal applications, PCM nanocomposite can act as a volumetric absorber. From the experiments, the PCMs were turned into a liquid stage; thus, steady state temperature mainly depended on the absorption ability of liquid PCM. In this research, the transmittance percentage was tested for wavelengths ranging from 250 nm to 2500 nm. To comprehend light transmission from the composites equated to solar spectrum data taken from NREI [51]. When comparing to solar spectral range, light transmission percentage of SH, SHM0.3, SHM0.5, SHM1.0, SHMS0.3, SHMS0.5, and SHMS1.0 were 62.71 %, 6.99 %, 7.69 %, 5.499 %, 7.7 %, 7.77 %, and 6.1 %, respectively. Moreover, the percentage reduction of samples was 88.8 %, 87.7 %, 91.15 %, 87.7 %, 87.6 %, and 90.27 %, respectively than salt hydrate PCM. It was apparent that the addition of MWCNT significantly reduced light transmission. Owing to this higher reduction of light transmission and increased absorption ability, these samples can be considered as attractive option for direct solar applications.

Similarly, the light transmission percentage of prepared FMWCNT nano-PCM composites were compared to the solar spectrum, as illustrated in Fig. 8(c) and (d). It was found that the percentage of transmission of prepared samples are 6.375 %, 5.73 %, 4.76 %, 22.17 %, 11.5 %, and 10.5 % for SHF0.3, SHF0.5, SHF1.0, SHFS0.3, SHFS0.5, and SHFS1.0, respectively; also, the percentage reductions of developed samples transmission were 89.83 %, 90.86 %, 92.41 %, 91.75 %, 91.56 %, and 91.22 %, respectively, than pure hydrate PCM. The maximum reduction was observed in FMWCNT dispersed salt hydrate PCM. From the discussion, it was evident that FMWCNT dispersed PCM composite
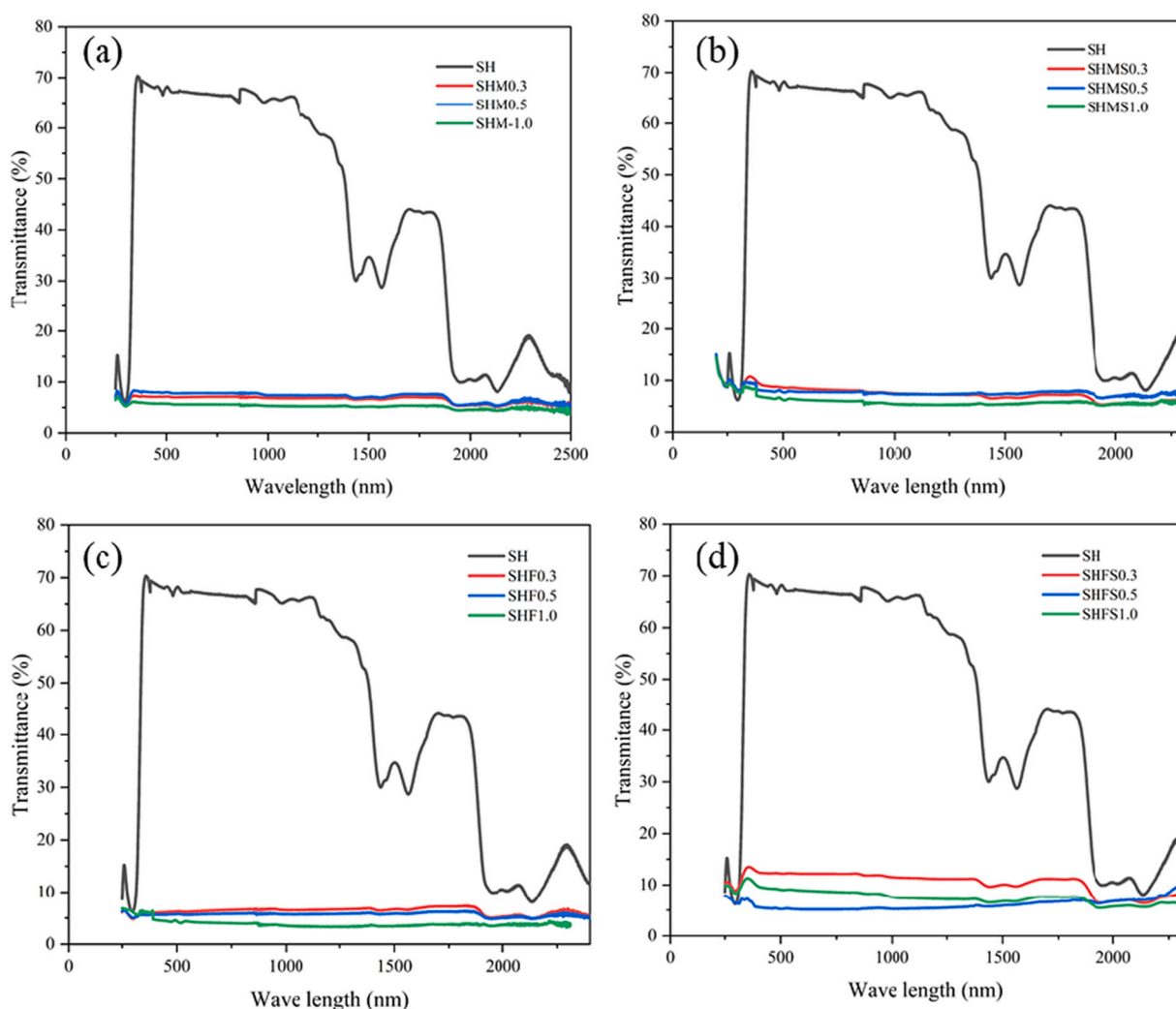

Fig. 8. Light transmission curve of (a) SHM, (b) SHMS, (c) SHF, (d) SHFS.

had higher reduction than other composite samples. The maximum reduction is observed at 1.0 wt% in all cases. It can be inferred that the amount of light absorbed depended on the weight percentage of NPs present in the salt hydrate PCM. Photo transmissibility of MWCNT, and FMWCNT dispersed PCM (with and without surfactant) composite decreased with a rise in weight concentrations of NPs, and the different weight concentrations of NePCM optical transmittance was less than the pristine PCM. From the above the discussion, it can be concluded that the addition of MWCNT/FMWCNT with and without surfactant, into the salt hydrate has good improvement in all the cases; also, there was no marked difference in terms of absorptivity with surfactant and without surfactant in the composite due to excellent dispersion stability, and the black color property of MWCNTs added in the composites. Due to increased absorption and reduction in transmission, the MWCNT /FMWCNT with salt hydrate PCM composite can be a suitable composite for solar thermal applications.

3.5. Thermal stability analysis

TGA (Perkin Elmer TGA-4000) is used to study the thermal decomposition performance of salt hydrate PCM, NePCM with and without surfactant with various concentrations of MWCNT and FMWCNT ranging from 0.3 to 1.0 wt% as shown in Fig. 9. From the EDX results, the element present in the salt hydrate may be Magnesium Nitrate hexahydrate ($Mg(NO_3)_2.6H_2O$). According to the literature, salt hydrate PCM decomposes into two stages. Stage one is freeing water molecules

around 290–300 °C; the second stage was decomposing of the remaining $Mg(NO_3)_2$; the remaining left is magnesium oxide (MgO) and carbon residues.

In the TGA graph, PCM begins to degrade around 64 °C, thereby contributing to a drop in 26.4 % mass by 151 °C, which related to loss in water ($5H_2O$); the remaining water particles were lost around 291 °C. The remaining mass was lost at around 455 °C, in this temperature, magnesium nitrate decomposed, and remaining left were 9.54 % which may be magnesium oxide (MgO) and residue of carbon. The percentage of mass that remained after 650 °C was 8.64 %, mainly containing carbon residue and oxides. TGA graph of base PCM with different concentrations of MWCNTs is displayed in Fig. 9(a). The starting and ending degradation temperature has significantly improved by the addition of MWCNT with PCM. The thermal degradation initiates at 69.1 °C, 67 °C, and 68.2 °C and ended at 459 °C, 461 °C, and 470 °C for SHM0.3, SHM0.5, and SHM.01, respectively. In first stage, water molecule reduction happened two steps; in first step, $5H_2O$ water molecules decomposed at 132.0 °C, 145.0 °C, and 140.0 °C and the weight reduction was 17.5 %, 18 %, and 20.4 %, respectively. The remaining water molecules (H_2O) decomposed at 298.0 °C, 276.0 °C, and 307.0 °C. Similarly, the weight concentrations of remains after degradation were 11.95 %, 14.66 %, and 12.08 %. After heating 650 °C, the percentage reduced to 10.0 %, 10.67 %, and 10.10 %, containing of carbon residues and some oxides. It is noticed that the decompose temperature increased after adding up nanoparticles to the PCM. Similarly, Fig. 9(b) shows the step-by-step decomposition temperature of MWCNT dispersed salt
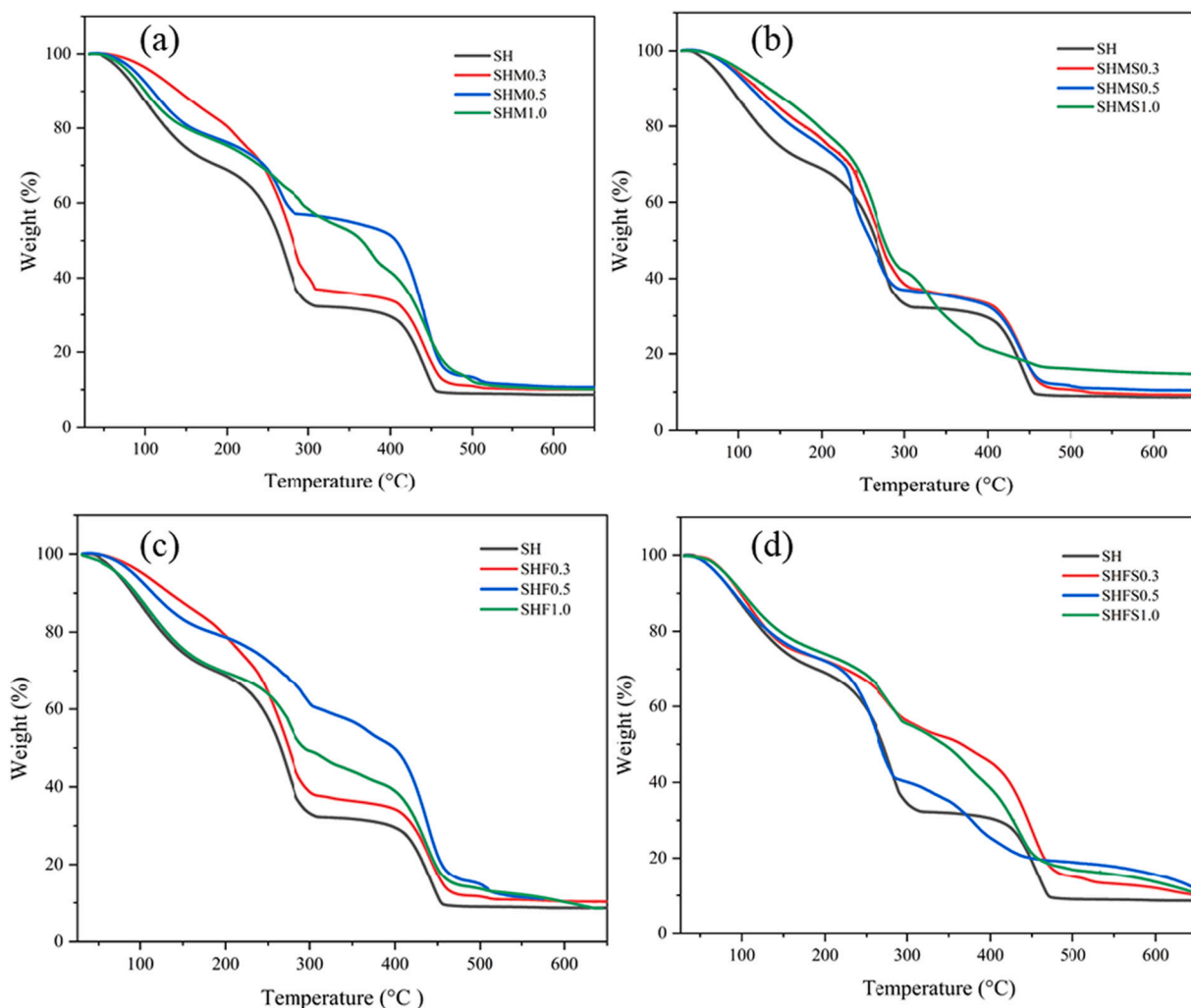

Fig. 9. Thermal stability curve of (a) SHM, (b) SHMS, (c) SHF (d) SHFS.

hydrate PCM with surfactant with various concentrations. The starting and ending degradation temperatures have noticeably increased by adding MWCNT and surfactant with SH PCM. The degradation began at 73.89 °C, 63.41 °C, and 76.9 °C and ended at 460 °C, 455 °C, and 433 °C for SHMS0.3, SHMS0.5, and SHMS1.0, respectively. The first step loss of weight at 165 °C, 152 °C, and 152 °C were 18.5 %, 18 %, and 23 %; this is due to $5H_2O$ water molecule freeing. The remaining H_2O water molecules loss were at 291 °C, 280 °C, and 283 °C, respectively. After decomposition the weight percentage of residues were 12.44, 13.0 %, and 17.0 %, respectively. Once heated 650 °C, the left mass percentage were 9.24 %, 10.47 %, and 14.7 % for SHMS0.3, SHMS0.5, and SHMS1.0, which consisted of carbon residues and some oxides.

Correspondingly, Fig. 9(c) shows the step-by-step decomposition temperature of FMWCNT dispersed salt hydrate PCM with various concentrations. The decomposition initiated at 75 °C, 70 °C, and 68 °C and ended at 459 °C, 461 °C, and 470 °C for SHF0.3, SHF0.5, and SHF1.0, respectively. The initial percentage mass reductions of 17 %, 17.3 %, and 20.4 % corresponding temperatures at 145 °C, 145.9 °C, and 142 °C, respectively, were due to the $5H_2O$ water molecules freeing. The remaining H_2O water molecules were freeing at 293 °C, 299 °C, and 307 °C, respectively. After decomposing the $Mg(NO_3)_2$, the remaining weight percentage were 12.96 %, 14.15 %, and 12.08 %. Similarly, Fig. 9(d) illustrates the step-by-step decomposition curve of FMWCNT and SDBS with PCM. The degradation started at 77.8 °C, 72.8 °C, and 69.1 °C and ended 471 °C, 458.2 °C, and 465 °C for SHFS0.3, SHFS0.5, and SHFS1.0, respectively. For the initial stage reduction weights of 22 %, 17 %, and 21.8 % corresponding temperatures are 153 °C, 141 °C, and 145 °C, due to freeing of $5H_2O$. The remaining water molecules were freeing at 297 °C, 293 °C, and 291 °C, respectively. After decomposing $Mg(NO_3)_2$ the weight percentage left was 13.2 %, 14.35 %, and 18.2 %, respectively. The developed NePCM composite onset temperatures were greater than the pure PCM, revealing its thermally stable. The enhancement in thermal stability could be ascribed to the thermal barrier creation between PCM and NPs. This formation of thermal barrier was because of accumulation of MWCNT, and FMWCNT particles may delay the breakage polymer chain to monomers; therefore, thermal stability increased [27]. This is due to the addition of MWCNT and FMWCNT NPs into the salt hydrate PCM. The thermal degradation happened at higher temperatures than salt hydrate PCM in all cases. This displayed that MWCNT and FMMWCNT with and without SDBS can extend the thermal stability of the PCM. A decrease or increase of stability depends on two reasons: first, one formation of the thermal barrier due to the adding MWCNT and second one creation of oxygen vacancy of NPs due to thermal excitation. The first one overshadows the increase in thermal stability and the second one overshadows the decrease in thermal stability.

From the above analysis, the initial degradation was delayed for MWCNT and FMWCNT with SDBS. The final decomposition was almost similar for all cases. In all cases, the final decomposition was increased, which implied the improvement in thermal stability. This was due to the presence of MWCNTs and FMWCNTs in the composite, which has exhibited excellent thermal stability. This stability of NePCM against the thermal decomposition contributed to the additional heat capacity.

3.6. Thermal conductivity analysis

The TC of the NePCMs mainly depended on the degree of dispersion of the NPs into the PCMs. The effective dispersion of nanoparticles depended on the length of stirring and the duration of ultrasonication of composite mixture. The TC was examined using Thermal Analyser (SH-03, METER) at ambient temperature with a percentage error of ±5 %. Fig. 10 shows the four different combinations of composite PCM with various weight percentage concentrations. The TC of pure salt hydrate was 0.46 $Wm^{-1} K^{-1}$, and it has been increased to 0.64 W/mK, 0.66 W/mK, and 0.64 W/mK for SHM0.3, SHM0.5, and SHM1.0 and the TC of salt hydrate with MWCNT and surfactant was 0.67 W/mK, 0.69 W/mK,
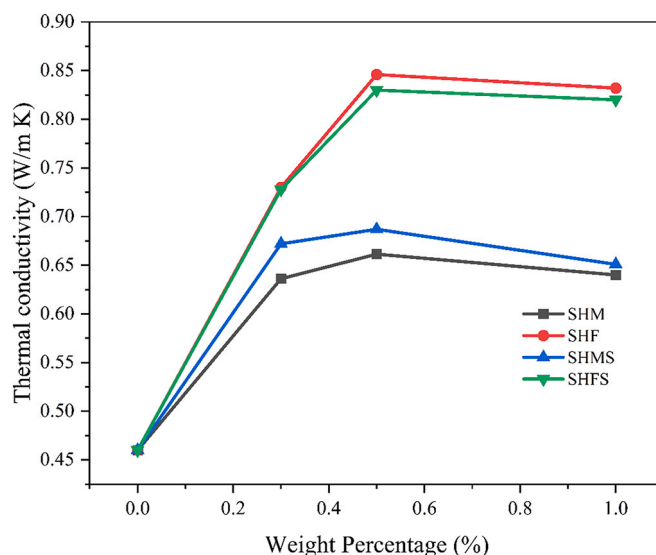
Fig. 10. Thermal conductivity of MWCNT, FMWCNT dispersed salt hydrate PCM with surfactant and without surfactant.

and 0.65 W/mK for SHMS0.3, SHMS0.5, and SHMS1.0, respectively.

It has been seen that the TC increased with an increase weight fraction of MWCNT, about 0.5 wt% and then decreased for higher concentrations for both samples. The decrement was due to the homogeneous mixture and agglomeration of NPs in the PCM. The agglomeration was the major reason for decreasing the TC as it leading to breaking the thermal network and reducing the TC or increasing the NPs scattering as the concentration increased. The dispersion of MWCNT in palmitic acid TC increased with a rise in the concentration of nanoparticles and the extreme increment was 67 % as described by Ji et al. [52] and increment of 60.5 % was reported by Manoj Kumar et al. [50]. M. Noori et al. [53] reported that the TC increased with an increase of nanoparticle concentration up to 3 wt% of CuO, then decreased. The percentage enhancement of SHM and SHMS were found to be 39.13 %, 43.48 %, 39.13 % and 45.65 %, 50.0 %, 41.3 % for 0.3, 0.5, and 1.0 wt%, respectively than pristine salt hydrate PCM. The maximum enhancement was 43.48 % and 50 % for SHM0.5 and SHMS0.5, respectively. It has to be noted that the incorporation of SDBS increased the intermolecular free mobility of particles, which made the NePCM more stable of MWCNTs, due to which the TC increased.

In addition, the TC of SHF were 0.73 W/mK, 0.85 W/mK, and 0.83 W/mK for SHF0.3, SHF0.5, and SHF1.0, respectively and the TC of SHFS were 0.72 W/mK, 0.83 W/mK, and 0.82 W/mK for SHFS0.3, SHFS0.5, and SHFS1.0, respectively. The percentage enhancement of SHF and SHFS were found to be 58.7 %, 84.78 %, 80.43 and 56.52 %, 80.4 %, 78.3 % for 0.3, 0.5, and 1.0 wt%, respectively than pristine salt hydrate PCM. The TC was increased with an increase of weight concentration up to 0.5 wt% then decreased for higher concentration for both cases. The reduction of TC may be due to the uneven dispersion, and the agglomeration of NPs in PCM can result in non-uniform composite formation due to which the TC is decreasing. In this case, after adding a surfactant, the TC was not improved because the functionalized MWCNTs are already having excellent stability in the base PCM. There is no need to use a surfactant to the FMWCNT dispersed PCM; it gave a negative impact on the composite PCM due to which the TC decreased [54].

The functionalized MWCNT has a higher TC, about 84.78 %, than all other cases, due to FMWCNT showing better dispersion than the pure MWCNT dispersed PCM. Surface modified functional group can generate a chemical bond between nanoparticle and PCM matrix; also, it can form a robust and rigid bond in the process of the PCM curing effect. There was a strong covalent bonding between MWCNT and PCM, forming a heat flow network that can decrease the larger number of

interfacial thermal network throughout the nano PCM; the addition of little amount of NPs enhances TC. Furthermore, there were two crucial factors for improving the TC of FMWCNT dispersed PCM; (i) Surface-modified MWCNT form a covalent bond between nanoparticles and PCM and it is a very important factor for enhancing the TC and (ii) the well dispersed and well compatibility of FMWCNT and PCM matrix; large MWCNT from the heat flow network, thereby have a higher TC due to external area of FMWCNT contact area.

On the other hand, most of the studies reported that the nanoparticle size of the MWCNTs directly impacts thermal performance [55]. In this research, it was observed that long-walled nanotubes have higher conductivity enhancement than short-walled MWCNTs. Moreover, the TC enhancement was non-linear to the weight % of NPs. This non-linearity was due to the random agglomeration and uneven dispersion of NPs when the weight % of NPs increased. The same pattern of the result was reported when the author used Al_2O_3 as a nanoparticle and paraffin as a PCM [56]. However, the maximum enhancement of TC of nano dispersed PCM was depending on the configuration of NPs, concentration rate, and dispersion of nanoparticles- they have to be prudently selected, and more attention to be paid to the solid phase PCM.

3.7. Thermal cycle test

Thermal cycling test was used to ensure the thermal reliability of formulated nanocomposites. A custom-made thermal cycler (Model: Labs Thermal Cycler Tester-AIBS) with three compartments to run three different samples at the same time was used to run the samples. The samples were placed in a crucible and a thermocouple electronically manipulated was inserted into the samples. The maximum temperature was set to be 70 °C, the temperature greater than melting temperature of the developed samples. The crucible was heated from below the crucible holder to achieve the maximum temperature. Once the maximum temperature was achieved the heater is automatically turn off, activating the cooling system of the cycler. A fan was used to cool the crucible and samples. Once the minimum temperature 30 °C was reached, the cooling system automatically turns off. The amount of 500 cycles sample taken was very small, so that the maximum temperature reached within 2 min and the cooling time was around 3 min. The thermal cycling was carried out with pure salt hydrate PCM, and SHMS0.5 composite PCM. The Table 2 shows the latent heat values and melting temperature of selected samples, and Fig. 11 shows the DSC graph of after and before thermal cycling of S50, and SHMS0.5 nanocomposites. The LH and melting temperatures of SH, and SHMS0.5 are 93.39 kJ/kg, 88 kJ/kg, and 49.6 °C, 50.1 °C, respectively for 0 cycle. The LH and melting temperature of SH, and SHMS0.5 were 100 kJ/kg, 84.35 kJ/kg and 52.1 °C, 51.9 °C, respectively for 500 thermal cycles. The LH was increased for SH and decreased for SHMS0.5 samples after 500 thermal cycling. The increasing latent heat may be attributed that the solid-solid transition region is absent in the heating cooling cycles; the absence of solid-solid transition due to the rearrangement of the molecules of the PCM composites. The decreasing latent heat may be attributed to the particle agglomeration caused by repeated phase changes of nanocomposite. Furthermore, the melting temperature was increasing in all cases after 500 thermal cycling. It is may the attributed the following reasons: (i) nanoparticles present in the sample, (ii) impurities in the sample, (iii)
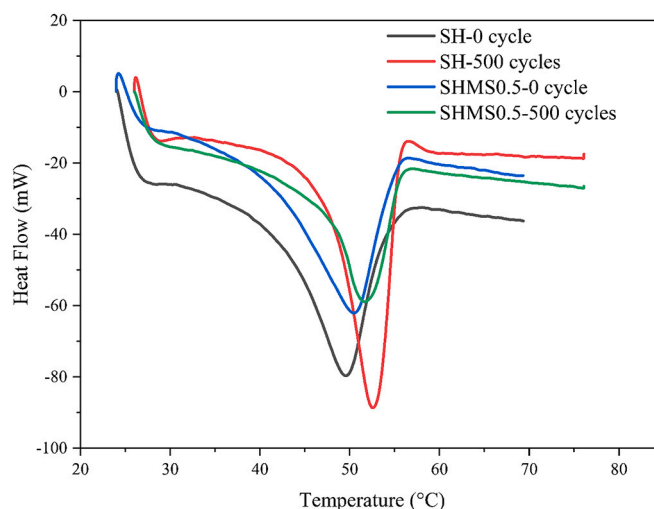
Fig. 11. DSC graph of SH, SHMS0.5 and SHF0.5 at 0 and 500 heating cooling cycles.

formation of C=C. In the case of SH, the NPs are not doped in SH PCM, therefore, the increase in temperature is may be the formation of C=C and the impurities present in the PCM. The Figs. 12 and 13 show the FTIR and TGA graphs of 500 heating cooling cycles of pure salt hydrate PCM, and S50MS0.5 composites, respectively. The FTIR spectrum graphs have revealed that there is no or additional functional groups were found, thus ensuring the prepared composite was chemically stable even after 500 thermal cycles; also, the TGA results displayed that the thermal decomposition-initiated onset temperatures of 64 °C, 66 °C, and ended at 478 °C, 468 °C for S50, and S50MS0.5 after 500 cycles. After the degradation, the weight percentage of residues was 10.3 %, and 10.34 %, respectively, mainly containing magnesium oxide and carbon residues. It was observed that the developed S50MS0.5 nanocomposite decomposition temperature was higher than base salt hydrate PCM. The stability of salt hydrate was increasing trend which may be due to the C=C formation; therefore it delayed the breakage of chain into the monomer. In the case of SHMS0.5 the stability was slightly reduced than SH after 500 cycling. The reduction may be due to the agglomeration of nanoparticles, due to that the thermal barrier effect reduced, so that the thermal stability reduced. Also, found that after 500 heating and cooling cycles the prepared nanocomposites are chemically and thermally stable, the melting enthalpy also slightly varied. The above discussion shows that the developed nanocomposites were excellent candidates for thermal energy storage applications.
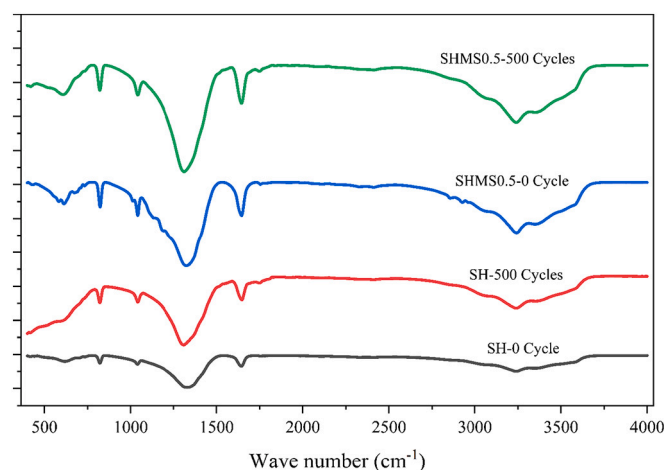
Table 2
Melting enthalpy and melting temperature of salt hydrate and optimum nanocomposite at 0 and 500 heating cooling cycles.

Composites	Latent heat (kJ/kg)		Melting point (°C)		Difference in LH (kJ/kg)	Difference in melting temperature (°C)
	0	500	0	500		
SH	93.39	100	49.6	52.1	6.61	2.5
SHMS0.5	88	84.35	50.1	51.9	−3.65	1.8

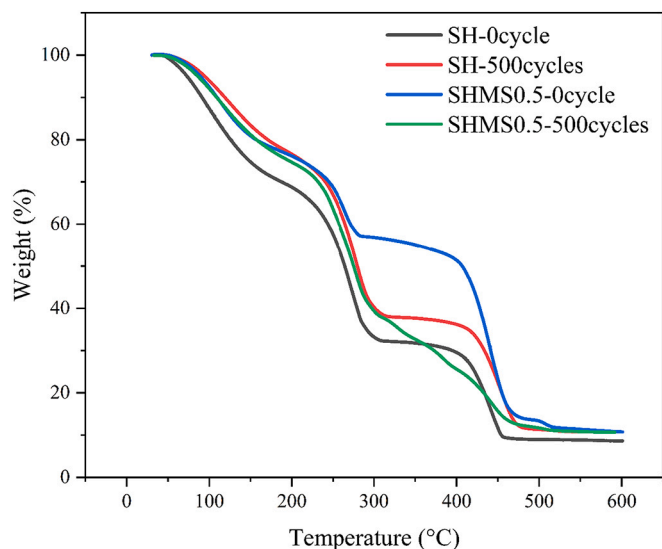**Fig. 12.** FTIR graph of SH, SHMS-0.5 and SHF-0.5 at 0 and 500 cycles.

Fig. 13. TGA graph of SH, SHMS-0.5 and SHF-0.5 at 0 and 500 cycles.

4. Conclusions

In this present work, MWCNT/FMWCNT dispersed salt hydrate PCM with and without surfactant was prepared, and thermophysical properties were investigated and the effect of surfactant was discussed thoroughly. The critical findings are enumerated as below:

The TEM images have shown the size of CNTs before and after functionalization; the size of MWCNT was noted between 10 and 20 nm, and prior to acid functionalization, the size of the MWCNT is slightly increased up to 31.1 nm; it confirmed the attachment of the -COOH group on the surface of the MWCNTs. The uniformity of dispersed CNTs, existing elements in the composites was confirmed by EDX analysis. The FTIR results have shown that the prepared nano PCM was physically well mixed, and no chemical action appeared in the developed composite PCM. The thermal conductivity of formulated SHMS0.3, SHMS0.5, SHMS1.0, SHF0.3, SHF0.5 and SHF1.0 was 0.67, 0.69, 0.65, 0.73, 0.85 and 0.83 $Wm^{-1} K^{-1}$, respectively. The thermal conductivity was enhanced up to 0.5 wt% after which there was a decreasing trend in all cases. The thermal conductivity was higher for SHMS0.5 by 50.0 % and SHF0.5 by 84.78 % than pure salt hydrate. The thermal conductivity was higher for the addition of surfactant with SH/MWCNT composites. The increase the intermolecular free mobility of particles made the NePCM more stable of MWCNTs. Furthermore, the thermal conductivity of SHF composites has higher thermal conductivity compared to all other composites. FMWCNT has shown better dispersion than the pure MWCNT dispersed PCM. Surface modified functional group can generate a chemical bond between nanoparticle and PCM matrix; also, it forms a strong and rigid bond in the process of the PCM curing reaction. The strong covalent bonding between MWCNT and PCM forms a heat flow network that can decrease the large number of interfacial thermal network throughout the nano PCM network, results increase the thermal conductivity.

The latent heat of formulated SHM0.3, SHM0.5, SHM1.0, SHF0.3, SHF0.5 and SHF1.0 was 98, 92, 78, 120, 97.22 and 78 kJ/kg, respectively. The LH was higher for a lower concentration of nanoparticles embedded into the salt hydrate PCM. The latent heat was increased up to 0.3 wt% concentration and afterwards, was showing a decreasing trend for SHM, SHF and SHFS composites. In this case, adding surfactant/stabilizer decreases the latent heat capacity for all cases. From the TGA result, the prepared composites had higher thermal stability than pure salt hydrate PCM. It has been found that composite without SDBS exhibited a higher thermal stability. The reduction of light transmission of prepared composites was 91.15 %, 92.41 %, 90.27 %, and 91.22 % for

SHM1.0, SHF1.0, SHMS1.0, and SHFS1.0, respectively than pure salt hydrate PCM. Further, it confirmed that SHMS and SHF had higher reductions in light transmission. In addition, it was revealed that the developed nanocomposites are stable up to 468 °C after 500 thermal cycling, revealing that the prepared nanocomposites could be used for long-term solar thermal energy storage applications. Thus, the FMWNT enhanced salt hydrate PCM had excellent thermal conductivity, LH, light absorption and thermal stability. In addition, MWCNT dispersed salt hydrate with surfactant nanocomposite PCM had better thermal conductivity, lower LH, better light absorption, excellent thermal stability, and good dispersion and chemical stability than MWCNT dispersed salt hydrate PCM.

Finally, functionalized MWCNTs enhanced nano PCMs has higher and excellent performance than other composite PCMs. In the future, the FMWCNT needs to be established in real-world solar thermal applications.

CRediT authorship contribution statement

Reji Kumar R: Data curation, Investigation, Formal analysis, Writing – original draft. **A.K. Pandey:** Conceptualization, Methodology, Formal analysis, Validation, Supervision, Project administration. **M. Samykano:** Validation, Writing – review & editing, Methodology, Supervision, Project administration. **Yogeshwar Nath Mishra:** Validation, Writing – review & editing. **R.V. Mohan:** Validation, Writing – review & editing. **Kamal Sharma:** Writing – review & editing. **V.V. Tyagi:** Validation, Writing – review & editing, Methodology.

Declaration of competing interest

The authors declare that they have no known competing financial interests or personal relationships that could have appeared to influence the work reported in this paper.

Data availability

Data will be made available on request.

Acknowledgements

References

[1] H.M.S. Al-Maamary, H.A. Kazem, M.T. Chaichan, Climate change: the game changer in the Gulf Cooperation Council Region, Renew. Sustain. Energy Rev. 76 (January) (2017) 555–576, https://doi.org/10.1016/j.rser.2017.03.048.

[2] K. Baz, et al., Asymmetric impact of fossil fuel and renewable energy consumption on economic growth: a nonlinear technique, Energy 226 (2021) 120357, https://doi.org/10.1016/j.energy.2021.120357.

[3] J. Yu, Y.M. Tang, K.Y. Chau, R. Nazar, S. Ali, W. Iqbal, Role of solar-based renewable energy in mitigating CO2 emissions: evidence from quantile-on-quantile estimation, Renew. Energy 182 (2021) 216–226, https://doi.org/10.1016/j.renene.2021.10.002.

[4] R. Reji Kumar, M. Samykano, A.K. Pandey, K. Kadirgama, V.V. Tyagi, Phase change materials and nano-enhanced phase change materials for thermal energy storage in photovoltaic thermal systems: a futuristic approach and its technical challenges, Renew. Sustain. Energy Rev. 133 (September) (2020), 110341, https://doi.org/10.1016/j.rser.2020.110341.

[5] A. Arshad, M. Jabbal, Y. Yan, Preparation and characteristics evaluation of mono and hybrid nano- enhanced phase change materials (NePCMs) for thermal management of microelectronics 205, 2020. August 2019.

[6] Z. Ling, J. Liu, Q. Wang, W. Lin, X. Fang, Z. Zhang, MgCl2·6H2O-Mg(NO3)2·6H2O eutectic/SiO2 composite phase change material with improved thermal reliability and enhanced thermal conductivity, Sol. Energy Mater. Sol. Cells 172 (3) (2017) 195–201, https://doi.org/10.1016/j.solmat.2017.07.019.

[7] K. Nagano, K. Ogawa, T. Mochida, K. Hayashi, H. Ogoshi, Performance of heat charge/discharge of magnesium nitrate hexahydrate and magnesium chloride hexahydrate mixture to a single vertical tube for a latent heat storage system, Appl. Therm. Eng. 24 (2–3) (2004) 209–220, https://doi.org/10.1016/j.applthermaleng.2003.09.002.

[8] Q. Xiao, J. Fan, Y. Fang, L. Li, T. Xu, W. Yuan, The shape-stabilized light-to-thermal conversion phase change material based on CH3COONa·3H2O as thermal energy storage media, Appl. Therm. Eng. 136 (2018) 701–707, https://doi.org/10.1016/j.applthermaleng.2018.03.053.

[9] X. Li, Y. Zhou, H. Nian, X. Zhang, Advanced nanocomposite phase change material based on calcium chloride hexahydrate with aluminum oxide nanoparticles for thermal energy storage Advanced nanocomposite phase change material based on calcium chloride hexahydrate with aluminum oxide nanopart, 2017.

[10] M.I. Hasan, H.O. Basher, A.O. Shdhan, Experimental investigation of phase change materials for insulation of residential buildings, Sustain. Cities Soc. 36 (April 2017) (2018) 42–58, https://doi.org/10.1016/j.scs.2017.10.009.

[11] N. Jamil, et al., A review on nano enhanced phase change materials: an enhancement in thermal properties and specific heat capacity, J. Adv. Res. Fluid Mech. Therm. Sci. 57 (1) (2019) 110–120.

[12] R.R. Kumar, Experimental investigations on thermal properties of copper (II) oxide nanoparticles enhanced inorganic phase change materials for solar thermal energy storage applications, 2022.

[13] B. Eanest Jebasingh, A. Valan Arasu, A comprehensive review on latent heat and thermal conductivity of nanoparticle dispersed phase change material for low-temperature applications, Energy Storage Mater. (2019), https://doi.org/10.1016/j.ensm.2019.07.031.

[14] R.K. R, M. Samykano, A.K. Pandey, K. Kadirgama, V.V. Tyagi, A comparative study on thermophysical properties of functionalized and non-functionalized Multi-Walled Carbon Nano Tubes (MWCNTs) enhanced salt hydrate phase change material, Sol. Energy Mater. Sol. Cells 240 (March) (2022) 111697, https://doi.org/10.1016/j.solmat.2022.111697.

[15] K. Kyriakidou, D. Brasinika, A.F.A. Trompeta, E. Bergamaschi, I.K. Karoussis, C. A. Charitidis, In vitro cytotoxicity assessment of pristine and carboxyl-functionalized MWCNTs, Food Chem. Toxicol. 141 (March) (2020) 111374, https://doi.org/10.1016/j.fct.2020.111374.

[16] O. Choi, S. Karki, R.R. Pawar, S. Hazarika, P.G. Ingole, A new perspective of functionalized MWCNT incorporated thin film nanocomposite hollow fiber membranes for the separation of various gases, J. Environ. Chem. Eng. 9 (1) (2021), 104774, https://doi.org/10.1016/j.jece.2020.104774.

[17] J.Y. LiuLiu, Jianlei Niu, Formulation of highly stable PCM nano-emulsions with reduced supercooling for thermal energy storage using surfactant mixtures, Sol. Energy Mater. Sol. Cells 223 (2021), 110983.

[18] S. Ranjbar, H. Masoumi, R. Haghighi Khoshkhoo, M. Mirfendereski, Experimental investigation of stability and thermal conductivity of phase change materials containing pristine and functionalized multi-walled carbon nanotubes, J. Therm. Anal. Calorim. 140 (5) (2020) 2505–2518, https://doi.org/10.1007/s10973-019-09005-x.

[19] M. Graham, E. Shchukina, P.F. De Castro, D. Shchukin, Mater. Chem. A (2016), https://doi.org/10.1039/C6TA06189C.

[20] M. Vivekananthan, V.A. Amirtham, Characterisation and thermophysical properties of graphene nanoparticles dispersed erythritol PCM for medium temperature thermal energy storage applications, Thermochim. Acta 676 (2019) 94–103, https://doi.org/10.1016/j.tca.2019.03.037.

[21] L.S. Wong-Pinto, Y. Milian, S. Ushak, Progress on use of nanoparticles in salt hydrates as phase change materials, Renew. Sustain. Energy Rev. 122 (July 2019) (2020) 109727, https://doi.org/10.1016/j.rser.2020.109727.

[22] A. Karaipekli, A. Biçer, A. Sarı, V. Veer, Thermal characteristics of expanded perlite/paraffin composite phase change material with enhanced thermal conductivity using carbon nanotubes, Energy Convers. Manag. 134 (2017) 373–381, https://doi.org/10.1016/j.enconman.2016.12.053.

[23] Y. Chen, Q. Zhang, X. Wen, H. Yin, J. Liu, A novel CNT encapsulated phase change material with enhanced thermal conductivity and photo-thermal conversion performance, Sol. Energy Mater. Sol. Cells 184 (May) (2018) 82–90, https://doi.org/10.1016/j.solmat.2018.04.034.

[24] A.K. Mishra, B.B. Lahiri, V. Solomon, J. Philip, Nano-inclusion aided thermal conductivity enhancement in palmitic acid/di-methyl formamide phase change material for latent heat thermal energy storage, Thermochim. Acta 678 (June) (2019), 178309, https://doi.org/10.1016/j.tca.2019.178309.

[25] S. Harikrishnan, S. Magesh, S. Kalaiselvam, Thermochimica acta preparation and thermal energy storage behaviour of stearic acid – TiO 2 nanofluids as a phase change material for solar heating systems, Thermochim. Acta 565 (2013) 137–145, https://doi.org/10.1016/j.tca.2013.05.001.

[26] A. Migdał-mikuli, E. Mikuli, R. Dziembaj, D. Majda, Ł. Hetma, in: Thermal decomposition of [Mg(NH 3)6](NO 3)2, [Ni (NH 3)6](NO 3)2 and [Ni (ND 3)6] (NO 3)2 419, 2004, pp. 223–229, https://doi.org/10.1016/j.tca.2004.01.035, no. 3.

[27] H. Masoumi, R. Haghighi khoshkhoo, S.M. Mirfendereski, Modification of physical and thermal characteristics of stearic acid as a phase change materials using TiO 2 -nanoparticles, Thermochim. Acta 675 (December 2018) (2019) 9–17, https://doi.org/10.1016/j.tca.2019.02.015.

[28] R. Daneshazarian, S. Antoun, S.B. Dworkin, International journal of heat and mass transfer performance assessment of nano-enhanced phase change material for thermal storage, Int. J. Heat Mass Transf. 173 (2021), 121256, https://doi.org/10.1016/j.ijheatmasstransfer.2021.121256.

[29] M.S. Kumar, V.M. Krishna, Experimental investigation on performance of hybrid PCM's on addition of nano particles in thermal energy storage, Mater. Today Proc. 17 (2019) 271–276, https://doi.org/10.1016/j.matpr.2019.06.430.

[30] C. Li, Q. Li, L. Cong, Y. Zhao, C. Liu, Y. Xiong, in: MgO based composite phase change materials for thermal energy storage: the effects of MgO particle density and size on microstructural characteristics as well as thermophysical and mechanical properties☆ 250, 2019, pp. 81–91, https://doi.org/10.1016/j.apenergy.2019.04.094 (April).

[31] A.R.Rupinder Pal Singh, Jia YinSze, S. CKaushik, Dibakar Rakshit, Thermal performance enhancement of eutectic PCM laden with functionalised graphene nanoplatelets for an efficient solar absorption cooling storage system, J. Energy Storage 33 (2021) 102092.

[32] Y. Zhou, et al., Multifunctional ZnO/polyurethane-based solid-solid phase change materials with graphene aerogel, Sol. Energy Mater. Sol. Cells 193 (December 2018) (2019) 13–21, https://doi.org/10.1016/j.solmat.2018.12.041.

[33] N. Gupta, A. Kumar, H. Dhasmana, V. Kumar, A. Kumar, Enhanced thermophysical properties of Metal oxide nanoparticles embedded magnesium nitrate hexahydrate based nanocomposite for thermal energy storage applications 32, 2020 no. April.

[34] X. Sun, L. Liu, Y. Mo, J. Li, C. Li, Enhanced thermal energy storage of a paraffin-based phase change material (PCM) using nano carbons, Appl. Therm. Eng. 181 (2020), 115992, https://doi.org/10.1016/j.applthermaleng.2020.115992.

[35] C.R. Raj, S. Suresh, V.K. Singh, R.R. Bhavsar, M. Chandrasekar, V. Archita, Life cycle assessment of nanoalloy enhanced layered perovskite solid-solid phase change material till 10000 thermal cycles for energy storage applications, J. Energy Storage 35 (December 2020) (2021) 102220, https://doi.org/10.1016/j.est.2020.102220.

[36] A. Al-Ahmed, A. Sarı, M.A.J. Mazumder, G. Hekimoğlu, F.A. Al-Sulaiman, Inamuddin, Thermal energy storage and thermal conductivity properties of Octadecanol-MWCNT composite PCMs as promising organic heat storage materials, Sci. Rep. 10 (1) (2020) 1–15, https://doi.org/10.1038/s41598-020-64149-3.

[37] S. Hashempour, M.H. Vakili, Preparation and characterisation of nano enhanced phase change material by adding carbon nano tubes to butyl stearate, J. Exp. Nanosci. 13 (1) (2018) 188–198, https://doi.org/10.1080/17458080.2018.1502480.

[38] K. Du, J. Calautit, Z. Wang, Y. Wu, H. Liu, A review of the applications of phase change materials in cooling, heating and power generation in different temperature ranges, Appl. Energy 220 (March) (2018) 242–273, https://doi.org/10.1016/j.apenergy.2018.03.005.

[39] R.K. R, et al., Phase change materials integrated solar desalination system: an innovative approach for sustainable and clean water production and storage, Renew. Sustain. Energy Rev. 165 (5) (2022), 112611, https://doi.org/10.1016/j.rser.2022.112611.

[40] K. B, A.K. Pandey, S. Shahabuddin, M. Samykano, T. M, R. Saidur, Phase change materials integrated solar thermal energy systems: Global trends and current practices in experimental approaches, J. Energy Storage 27 (November 2019) (2020) 101118, https://doi.org/10.1016/j.est.2019.101118.

[41] B.R. Anupam, U.C. Sahoo, P. Rath, Phase change materials for pavement applications: a review, Constr. Build. Mater. 247 (2020), 118553, https://doi.org/10.1016/j.conbuildmat.2020.118553.

[42] J. Jaguemont, N. Omar, P. Van den Bossche, J. Mierlo, Phase-change materials (PCM) for automotive applications: a review, Appl. Therm. Eng. 132 (2018) 308–320, https://doi.org/10.1016/j.applthermaleng.2017.12.097.

[43] M.M. Islam, M. Hasanuzzaman, N.A. Rahim, A.K. Pandey, M. Rawa, L. Kumar, Real time experimental performance investigation of a NePCM based photovoltaic thermal system: an energetic and exergetic approach, Renew. Energy 172 (2021) 71–87, https://doi.org/10.1016/j.renene.2021.02.169.

[44] V.T. Le, C.L. Ngo, Q.T. Le, T.T. Ngo, D.N. Nguyen, M.T. Vu, Surface modification and functionalization of carbon nanotube with some organic compounds, Adv. Nat. Sci. Nanosci. Nanotechnol. 4 (3) (2013) 2–7, https://doi.org/10.1088/2043-6262/4/3/035017.

[45] M. Morsy, M. Helal, M. El-Okr, M. Ibrahim, Preparation, purification and characterization of high purity multi-wall carbon nanotube, Spectrochim. ActaA Mol. Biomol. Spectrosc. 132 (2014) 594–598, https://doi.org/10.1016/j.saa.2014.04.122.

[46] F.A. Abuilaiwi, T. Laoui, M. Al-Harthi, M.A. Atieh, Modification and functionalization of multiwalled carbon nanotube (MWCNT) via Fischer esterification, Arab. J. Sci. Eng. 35 (1 C) (2010) 37–48.

[47] S.Y.W.H. Wang, S.X.D.S. Zhu, in: An investigation of melting/freezing characteristics of nanoparticle-enhanced phase change materials, 2012, pp. 1127–1131, https://doi.org/10.1007/s10973-011-2080-x.

[48] S. Harikrishnan, S. Imran Hussain, A. Devaraju, P. Sivasamy, S. Kalaiselvam, Improved performance of a newly prepared nano-enhanced phase change material for solar energy storage, J. Mech. Sci. Technol. 31 (10) (2017) 4903–4910, https://doi.org/10.1007/s12206-017-0938-y.

[49] L. Colla, L. Fedele, S. Mancin, L. Danza, O. Manca, Nano-PCMs for enhanced energy storage and passive cooling applications, Appl. Therm. Eng. 110 (2017) 584–589, https://doi.org/10.1016/j.applthermaleng.2016.03.161.

[50] P. Manoj Kumar, et al., Thermal characteristics analysis of a phase change material under the influence of nanoparticles, Mater. Today Proc. 45 (2021) 7876–7880, https://doi.org/10.1016/j.matpr.2020.12.505.

[51] C.A. Gueymard, The sun's total and spectral irradiance for solar energy applications and solar radiation models, Sol. Energy 76 (4) (2004) 423–453, https://doi.org/10.1016/j.solener.2003.08.039.

[52] P. Ji, H. Sun, Y. Zhong, W. Feng, Improvement of the thermal conductivity of a phase change material by the functionalized carbon nanotubes, Chem. Eng. Sci. 81 (2012) 140–145, https://doi.org/10.1016/j.ces.2012.07.002.

[53] M.M. Noori, H. Ali, M. Arjmand, S.H. Jafari, in: Paraffin/CuO nanocomposites as phase change materials: effect of surface modification of CuO, 2019, pp. 1–9, https://doi.org/10.1002/pc.25298, no. March.

[54] T. Boldoo, J. Ham, H. Cho, Comparison study on photo-thermal energy conversion performance of functionalized and non-functionalized MWCNT nanofluid, Energies 12 (19) (2019), https://doi.org/10.3390/en12193763.

[55] T. Wu, et al., Preparation of a low-temperature nanofluid phase change material: MgCl2–H2O eutectic salt solution system with multi-walled carbon nanotubes (MWCNTs), Int. J. Refrig. 113 (2020) 136–144, https://doi.org/10.1016/j.ijrefrig.2020.02.008.

[56] N.H. Mohamed, F.S. Soliman, H. El Maghraby, Y.M. Moustfa, Thermal conductivity enhancement of treated petroleum waxes, as phase change material, by A nano alumina: energy storage, Renew. Sustain. Energy Rev. 70 (October 2015) (2017) 1052–1058, https://doi.org/10.1016/j.rser.2016.12.009.